A. Spinelli, G. Cammi, C.C. Conti, S. Gallarini, M. Zocca, F. Cozzi, P. Gaetani, V. Dossena, A. Guardone
Experimental Observation and Thermodynamic Modeling of Non-Ideal Expanding Flows of Siloxane MDM Vapor for ORC Applications
Energy, Vol. 168, 2019, p. 285-294
doi:10.1016/j.energy.2018.11.071

Experimental observation and thermodynamic modeling of non-ideal expanding flows of siloxane MDM vapor for ORC applications

Andrea Spinelli[a,*], Giorgia Cammi[a], Camilla Cecilia Conti[b], Simone Gallarini[a], Marta Zocca[b], Fabio Cozzi[a], Paolo Gaetani[a], Vincenzo Dossena[a], Alberto Guardone[b]

[a]*Politecnico di Milano, Energy Department, via Lambruschini 4, 20156, Milano, Italy*
[b]*Politecnico di Milano, Aerospace Science and Technology Department, via La Masa 34, 20156, Milano, Italy*

Abstract

This paper reports extensive experimental results characterizing the supersonic expansion of an organic vapor in non-ideal thermodynamic conditions typical of organic Rankine cycle (ORC) turbines. Data are also employed to assess the accuracy of different thermodynamic models used to describe non-ideal expansions.

Experiments were carried out on a converging-diverging nozzle test section, where siloxane vapor MDM expanded in the proximity of the saturation curve, the typical operating region of ORC expanders, thus proving the importance of the present investigation for ORC technology. Indeed, detailed experimental data representative of ORC expansions, useful for design tool assessment, were lacking in the open literature up to date.

Two nozzles, featuring exit Mach number of 2.0 and 1.5, were tested from highly non-ideal states to dilute gas conditions. The nozzle flow was characterized by measuring total pressure, total temperature and static pressure along the axis. The Mach number was measured at the centerline through schlieren imaging. Vapor expansion was found to be dependent on inlet conditions, thus proving the flow non-ideality.

State-of-the-art thermodynamic models proved their capability of fully describing the flow non-ideality, while simpler and easier to implement equations of state, such as van der Waals, can be acceptable for preliminary expander calculations.

Keywords: Experiments in non-ideal compressible flows, Non-ideal supersonic expanding flows, Siloxane MDM, Test Rig for Organic Vapors, TROVA, ORC power systems.

---

*Corresponding author.
Email address: andrea.spinelli@polimi.it (Andrea Spinelli)

1. Introduction

Nowadays organic Rankine cycle (ORC) power systems represent a cost effective and mature technology for efficient power generation in the range of 100 kW to 100 MW in cases where thermal power is available at low to medium temperature. This is the case of renewable energy sources, such as geothermal reservoirs and biomass combustion, and heat recovery from industrial processes (power plants, cement factories) [1, 2]. In these power and temperature ranges, ORCs are preferred over steam Rankine cycles due to their relatively high efficiency and the simplicity of cycle configuration.

The expander is certainly a key element of an ORC system. Its efficiency has a significant impact on the whole cycle performance. At present, turbomachines are most commonly employed, being the use of volumetric expanders limited to mini or micro-ORCs and to low temperature applications [1]. Current design, optimization and analysis tools for ORC turbo-expanders are based on CFD codes [3, 4, 5] embedding state-of-the-art thermodynamic models [6, 7, 8]. These are necessary since the expansion process occurs, for a significant portion, through thermodynamic regions close to the vapor saturation curve and the critical point, where the vapor behavior is far from ideality.

Detailed experimental data focusing on typical turbine channel flows, which are key to assess the accuracy of such tools, are not available in the open literature up to date. Investigation within industrial turbines is impracticable, due to the limited accessibility of turbine stages and the unavailability of proper instrumentation. Thus, in recent years, many experimental facilities were conceived and designed in order to fill this gap in literature. At TU Delft, the Flexible Asymmetric Shock Tube (FAST) was built and operated to study fundamentals of wave propagation in dense vapor of organic compounds by exploiting a Ludwieg tube [9]. The main purpose of the facility is to provide experimental proof of non-classical gas-dynamic behavior of complex vapors in the single phase region close to the saturation curve and the critical point.

Concerning, more specifically, the study of expansions of complex fluid vapors in the non-ideal gas regime, other experimental activities are underway. The Test Rig for Organic VApors (TROVA) [10, 11, 12] at the Laboratory of Compressible fluid-dynamics for Renewable Energy Application (CREA) of Politecnico di Milano, is a blow-down operated facility built with the aforementioned purpose of contributing to the available bibliography concerning experimental data on ORC turbine flows. More generally, the aim is to also carry out fundamental research in the field of Non-Ideal Compressible Fluid Dynamics (NICFD), the branch of fluid-dynamics dealing with compressible flows whose behavior cannot be described by the ideal gas law. The TROVA test section can be equipped with planar nozzles, designed for different fluids and/or operating conditions, and it can also accommodate linear blade cascades. A converging-diverging nozzle is undoubtedly the simplest geometry that allows to expand vapor from subsonic to supersonic velocity, similarly to ORC turbine channels. Also, the use of a straight axis nozzle allows flow field investigation with the use of pressure taps-line-transducer systems, with no need of employing directional pressure probes, which are still unavailable for such unconventional flows. Moreover, the investigation of the flow within such nozzles or around aerodynamic and bluff bodies, represent themselves key fundamental NICFD experiments which are relevant for ORC applications [13, 14].

Continuous operation facilities are currently under commissioning. The ORCHID at TU Delft [15] implements a high-temperature regenerative ORC power system for components testing. The CLOWT at Muenster University of Applied Sciences [16] is a continuous ORC vapor tunnel designed and built to develop loss correlations for turbo-expanders by studying the flow through linear blade cascades up to transonic velocities.

This article extends the results of an experimental campaign performed on the TROVA nozzle presented in [17] by reporting findings for more non-ideal thermodynamic conditions. In addition, the reliability of different thermodynamic models in predicting the flow behavior is assessed against experimental data. Siloxane MDM (octamethyltrisiloxane, $C_8H_{24}O_2Si_3$) was selected as working fluid since it is largely employed in high temperature ORCs and it features a wide non-ideal thermodynamic region in the vapor phase where ORC expanders typically operate [18]. Two nozzles were employed; they were designed [19] to obtain a uniform Mach number of 2.0 and 1.5 at the outlet section, which are typical values for ORC turbine vanes, especially for initial stages. The two nozzles are operated at inlet conditions varying from highly non-ideal states to almost ideal gas conditions, namely for compressibility factor $Z = Pv/RT$ ranging between 0.63 and 0.98; P is the pressure, v the specific volume per unit mass, R the gas constant and T the temperature. The vapor flow is characterized by means of total pressure and total temperature measurements in a settling chamber upstream of the nozzle and by wall static pressure measurements along the nozzle center line. The schlieren technique is also applied to visualize the two-dimensional density gradient field along the axis direction. This enables the visualization of Mach waves in the diverging portion and thus the direct measurement of the Mach number at the axis.

Different tests, performed in similar conditions, exhibited good repeatability as proved by the obtained comparable results. Therefore, results are discussed here for two tests only, while details on the full experimental campaign, including the complete dataset and comparison with air operated nozzles, can be found in [20]. In particular, non-ideal compressible flow effects in the expansion process are highlighted in the following by referring to the influence of inlet conditions, which is absent in the case of polytropic ideal gas (PIG). The comparison of measured flow features with those calculated by modeling MDM vapor as a PIG in CFD simulations showed significant deviation from the ideal behavior. This proves the importance of accounting for non-ideal effects in the detailed design and performance prediction of ORC turbo-expanders and of any system operating with such unconventional compressible flows. On the other hand, isentropic expansion calculations were performed using equations of state of different complexity. The van der Waals model and the Helmoltz energy based equation of state developed by Span and Wagner [6] and implemented in RefProp [21, 22] are applied. Results obtained showed that the accuracy of the van der Waals model in predicting non-ideal effects can be considered sufficient for preliminary thermodynamic expander design and for the definition of turbo-expander configuration.

The paper is structured as follows. Section 2 describes the facility and the implemented measurement techniques, while section 3 presents the test procedure. Results are discussed in section 4, thermodynamic modeling of non-ideal flows is reported in section 5, and section 6 finally draws the conclusions.

2. Experimental apparatus and instrumentation

The TROVA is a batch-operated facility. The organic fluid under scrutiny is heated in a High Pressure Vessel (HPV) with constant volume in order to reach saturated, superheated, or supercritical conditions at pressure and temperature above the stagnation conditions at which the nozzle test section is fed. The opening of a fast operating Main Control Valve (MCV) allows the vapor to expand in a converging-diverging nozzle and to be then discharged to a Low Pressure Vessel (LPV) where de-superheating and condensation occur. The loop is closed by pumping the liquid to the HPV through a membrane pump. A more detailed description of the apparatus is given in [10, 12].

The plant is conceived to test a wide class of organic fluids at different operating conditions; therefore, the TROVA test section can accommodate different, specifically designed nozzles [19]. A planar configuration was preferred to easily equip the test section with an optical access. In case the nozzle operates in under-expanded or adapted conditions, the flow at the core can be assumed as isentropic and the pressure field at the axis can be measured without the use of calibrated pressure probes, which are currently not available. The experimental campaign was carried on two different nozzles. The first one, labeled M2.0, is designed to deliver a uniform flow at the exit with Mach number $M = 2.0$. A backward facing step of height h =0.1 mm (1.2% of the throat semi-height H) is machined at the geometrical throat to study the formation of oblique shocks downstream the separation point; details are given in [14]. The second nozzle, labeled M1.5, provides a uniform outlet flow at Mach number $M = 1.5$. It is machined with no step at the throat and an increased roughness at the profile surface, in order to promote the formation of weak waves, whose slope relative to the flow direction provide a direct measurement of the local Mach number. Along the axis, nine static pressure taps are located on the back plate, which is made of carbon steel and is mirror polished to perform schlieren visualization with a double passage arrangement. Available taps are labeled from 1 to 9 in the flow direction and have a diameter of 0.3 mm. A 30 mm-long line connects each tap with a piezo-resistive pressure transducer which measures the static pressure P at the tap location. Frontally, a planar quartz window provides optical access to the flow within the test section.

Nozzle total pressure P_T and temperature T_T are measured in the plenum upstream of the test section, where the flow velocity is about 1 m/s. This allows to measure P_T with a wall pressure tap. T_T is obtained by using two thermocouples. A first one of K type, labeled TCK, features a hot junction of 0.25 mm diameter. A second one of J type, labeled TCJ, exhibits a hot junction of 0.7 mm diameter. The distance between the two thermocouples is about 200 mm and the hot junctions are both located at the chamber axis. A two-sensor characterization method [23] was used to evaluate the thermocouple time constants $\tilde{\tau}$, which resulted in values of $\tilde{\tau}_{TCK} = 0.28$ s and $\tilde{\tau}_{TCJ} = 1.34$ s for TCK and TCJ respectively. The acquired signals exhibit a considerably low frequency content (e.g. for pressure signals about 99.995% of the energy content lies below 0.2 Hz), therefore no compensation was applied, since the reconstructed temperature featured a deviation well below the thermocouple expanded uncertainty, which is of 1 °C. Consistent (though more optimistic) time constant estimations were obtained by applying a theoretical model based on forced convection correlations (see [24, 25]).

Pressure sensors operate at temperature up to 343 °C and feature an undesired sensitivity to temperature changes. Therefore, a pressure-temperature calibration surface was built in a domain extended from 1 bar to full scale (FS $\in [3.5, 40$ bar]) for pressure and from 25 to 300 °C for temperature. This temperature range was also adopted for thermocouple calibration. The expanded uncertainty resulting from the calibration process is about 0.07% of the full scale for pressure sensors and about 1 °C for thermocouples. The dynamic response of the pressure measurement system, was assessed employing a viscous model capable of treating complex line-cavity systems [26]. A satisfactory value of about 200 Hz was estimated for the tap-transmission line resonance frequency.

The density gradient field was acquired through schlieren visualization technique. A digital trigger allowed to synchronize the acquired images with pressure and temperature measurements. A double passage schlieren system equipped with a 100 W Hg arc-lamp and a high speed CMOS camera was adopted. The camera sensor features an area of 11.34 x 7.12 mm and a resolution of 1936 $\times$ 1216 pixels. The knife edge arrangement is such that axial density gradients within the nozzle are visualized as dark areas if positive (compression waves) and bright regions if negative (expansion waves). A more detailed description of the instrumentation can be found in [27, 28].

3. Test methodology

Different experimental runs were performed on MDM vapor expanding through the two nozzles, M2.0 and M1.5, starting at highly non-ideal thermodynamic conditions close to the saturation curve. Indeed, the MDM vapor exhibits a small degree of superheating, with initial total conditions of $P_T \simeq 9$ bar and $T_T \simeq 270$ °C, corresponding to a minimum value of compressibility factor $Z_T \simeq 0.63$ and to reduced conditions of $P_{Tr} = P_T/P_C \simeq 0.63$ and $T_{Tr} = T_T/T_C \simeq 0.96$, where P_C and T_C are critical pressure and temperature respectively. A good repeatability was verified, therefore only one test for each nozzle is thoroughly discussed here. According to the nozzle name these two test are referred to as test M2.0 and test M1.5. For Mach measurements only, results are also shown for a second test with nozzle M1.5, which is labeled M1.5'.

Table 1: Total pressure P_T and temperature T_T, total compressibility factor Z_T, adapted nozzle expansion ratio β and exit Mach number M_{out} at time $t = 0$ s. The adapted nozzle expansion ratio β is defined as the total pressure P_T to outlet static pressure P_{out} ratio in adapted nozzle condition.

Test	$\mathbf{P_T}$ **(bar)**	$\mathbf{T_T}$ **(°C)**	$\mathbf{Z_T}$	$\beta = P_\mathbf{T}/P_\mathbf{out}$	$\mathbf{M_{out}}$
M2.0	9.02	269	0.65	9.16	2.03
M1.5	9.20	268	0.63	3.12	1.50

A single test run starts at the opening of the MCV, establishing the vapor flow within the nozzle, and lasts about 140 s, excluding the transient time related to the valve opening. The test ends when the nozzle flow reaches adapted/overexpanded conditions. The MCV is fully opened, thus the inlet total pressure and the flow rate through the nozzle are not controlled. Therefore, after the MCV opening transient lasting about 2 s, the total pressure decreases due to the HPV emptying and different thermodynamic states (from highly non-ideal to almost ideal ones) are obtained at the test section inlet. The emptying process of the HPV exhibits a relaxation time which is two orders of magnitude larger than the nozzle one [10, 12]. Measurements sampling frequency is as high as 1 kHz, for both pressure and temperature data, while the exposure time of schlieren imaging is 1 ms. Therefore, a steady flow within the nozzle is assumed at any time during the test.

The schlieren imaging acquisition rate is 20 fps (frame per second) and a synchronization with pressure and temperature data is obtained by buffering and averaging data in sets of 50 points, thus providing a final time resolution of 50 ms.

During each test run the nozzle always operates in under-expanded conditions, allowing to make the hypothesis of a large isentropic flow core (except in the wall proximity) as confirmed by CFD simulations [14]. Table 1 reports test conditions at the most non-ideal state (minimum total compressibility factor Z_T) occurring at time $t = 0$ s.

The temperature - specific entropy ($T - s$) diagram in Figure 1 shows the evolution of inlet conditions (P_T, T_T) during test M2.0, clarifying that as P_T is reduced, Z_T increases and ideal conditions are approached. Total temperature T_T does not exhibit a monotonic decreasing trend, reasonably due to a temperature non-uniformity between the HPV and the pipeline upstream of the nozzle at the beginning of the test. These trends in P_T, T_T and Z_T were observed during all experimental runs, including test M1.5. Corresponding diagrams for the latter test are not shown here for brevity. Figure 1 also allows to appreciate the extent of the explored thermodynamic region, as well as the proximity to the saturation curve. The specific entropy s and the compressibility factor Z were calculated as a function of P_T and T_T using the RefProp model for MDM. Also, three selected steady expansions occurring through nozzle M2.0 are represented as lines. These correspond, as illustrated in Figure 2, to pressure trends along

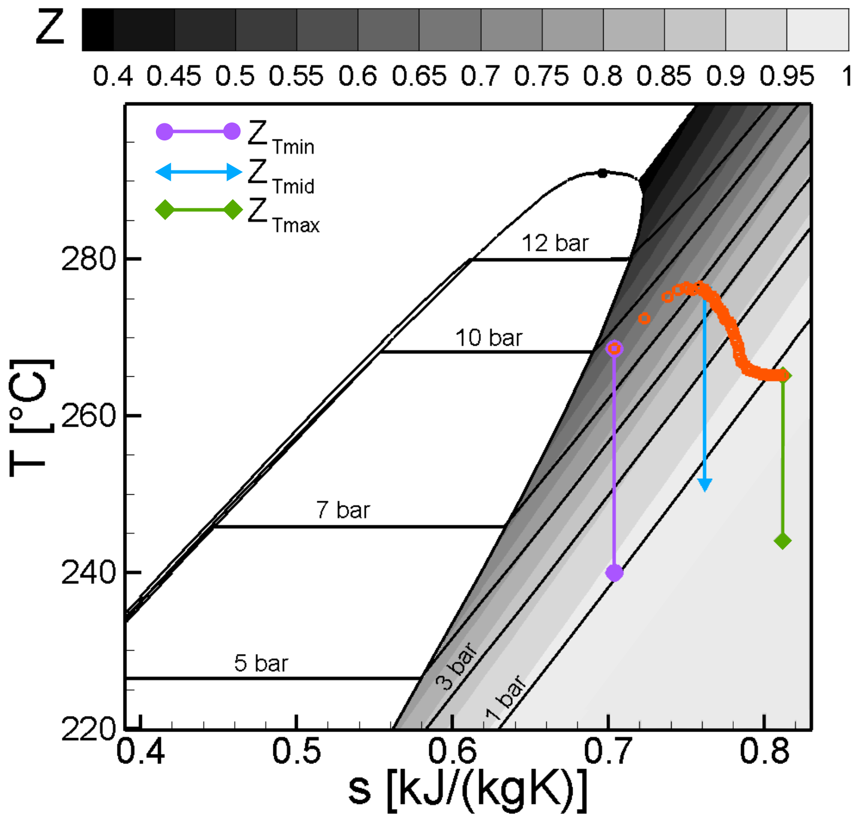

Figure 1: Explored thermodynamic regions for test M2.0. The time evolution of total conditions is plotted (orange dots) with a time step of 3 s. Steady isentropic expansions through the nozzle (lines) are also represented at three selected instants, corresponding to different total compressibility factors $Z_{Tmin} = 0.65$, $Z_{Tmid} = 0.80$, and $Z_{Tmax} = 0.98$. The specific entropy s and the compressibility factor Z are calculated using the RefProp model for MDM.

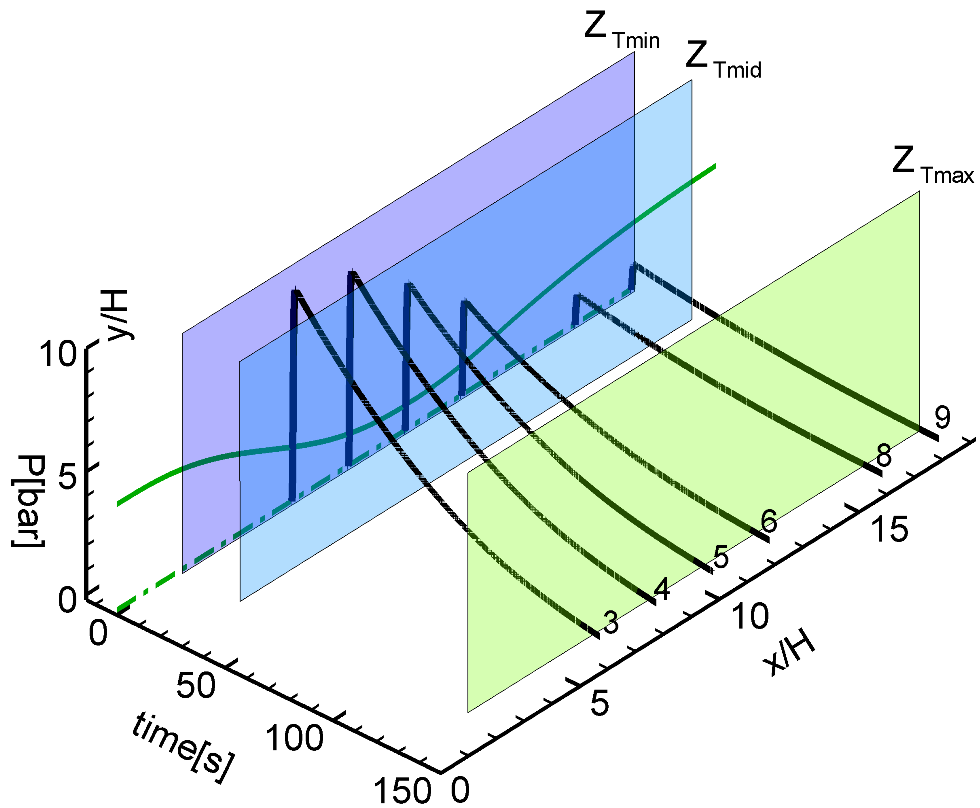

Figure 2: Time evolution of measured static pressure along the nozzle axis for test M2.0. Pressure tap position is explicited along the non-dimensional axial coordinate x/H; H is the nozzle semi-height at throat. The nozzle profile (green line) is sketched for clarity at a $t = 0$ s plane with y/H specifying the non-dimensional coordinate normal to the axis. Taps 1, 2 and 7 are not active. Cutting planes intersect the pressure signals at instants corresponding to the selected Z_T, thus showing the nozzle pressure trend for expansions depicted in Figure 1.

the nozzle axial coordinates extracted at significant time instants during the experimental run. Pressure along the nozzle decreases due to the vapor expansion while pressure at each tap along the nozzle decreases as the test proceeds due to the reduction of total pressure. Static pressure signals are labeled according to the corresponding tap numbers (from 1 to 9) which increase from nozzle inlet to outlet; tap number 5 is located at the geometrical throat.

4. Experimental results and comparison with CFD simulations

Experimental results are presented here for the two analyzed tests by discussing the steady nozzle expansions at different levels of non-ideality, marked by the value of the compressibility factor at total conditions, Z_T. The discussion is based on the analysis of the measured local pressure ratio P/P_T along the nozzle axis and on the Mach number distribution at the centerline of the diverging portion, as obtained by Mach lines detected through schlieren visualizations. Only measured quantities are therefore employed in the analysis. However, the calculated values of Z_T are also reported in order to highlight the level of non-ideality of different observed flows, while the compressibility factor Z along the expansion is computed to indicate the portion of the expansion process where non-ideal effects play a role. Finally, a comparison of experimental data with CFD results is presented to verify the accuracy of the numerical tool and of the implemented thermodynamic model. Two-dimensional (2D) CFD simulations, based on the Reynolds-averaged Navier-Stokes (RANS) equations, complemented with the Spalart-Allmaras turbulence model, were carried out using the SU2 suite [29, 3, 14]. The solver is coupled with the state-of-the-art multiparameter Helmoltz energy thermodynamic model [21] and the transport property model described in [30]. Both models are implemented in the RefProp library [22]. Consistently with the nozzle regime during the test (underexpanded or adapted, see section 3), the computational domain is limited to the converging-diverging nozzle and a quadrilateral grid is used. The first grid point is placed in the viscous sublayer, so that no wall functions are used. All details concerning CFD simulations can be found in [14].

4.1. Non-ideal pressure distribution

Steady nozzle expansions observed at variable non-ideal conditions and are presented here for the considered tests. Instants of interest are selected to clearly distinguish among different levels of non-ideality during the experimental run. Therefore, five instants featuring well distinct Z_T values, are selected in the minimum to maximum interval, namely $Z_T \in [0.65, 0.98]$ for test M2.0 and $Z_T \in [0.63, 0.98]$ for test M1.5. The selected Z_T values are reported in figure 3 and figure 4. For all conditions, the flow at the centerline is assumed to be isentropic, as discussed in section 3.

For each test, on the top of figure 3 and figure 4 a non-dimensional sketch of the nozzle is reported, completed with the axis line static pressure taps. Six out of nine taps were used for test M2.0, while four taps were available for test M1.5. In both cases active taps fall within the region of higher gradients.

The nozzle axial coordinate x is normalized by factor H, the nozzle semi-height at the throat, located at $x/H = 10.29$. The nozzle contour is plotted on the schlieren images of the MDM vapor flow acquired at time $t = 4.75$ s (Z_T=0.70) for test M2.0 and at time $t = 1.6$ s (Z_T=0.65) for test M1.5. They correspond to the minimum values of compressibility factor Z_T at which good quality images were acquired. Schlieren images at test start are not readable since at this time (namely at the highest non-ideal conditions) the light deviation due to the high flow density and compressibility is so high as to exceed the system measuring range. Positive density gradients are correctly visualized as dark areas, while negative density gradients, expected to be bright, are not so. These measuring range issues decrease as the test proceeds, so as more ideal conditions are approached. A more detailed discussion can be found in [31].

For test M2.0, the recessed step machined at the throat produces peculiar flow structures, which are only partially visible in the schlieren image of figure 3 but are well visible and thoroughly described in [17] for moderate non-ideal conditions. Oblique shock waves arise from the step at each profile, perturbing the flow at the axis only locally. Moreover, they occur at low Mach number $M \simeq 1.2$, and are therefore so weak that they cause a negligible reduction in total pressure, as proven for air in [27] and by numerical simulations for MDM. Hence, the flow can be assumed as isentropic at the nozzle axis with a constant total pressure P_T at all times. The flow is also isentropic at the centerline of nozzle M1.5, which features a smooth geometry, and Mach waves originated by the profile roughness are visible in the divergent portion. The nozzle operates in under-expanded conditions, as proven by the post-expansion structures (fans and slip lines) distinguishable at the exit section, which is included in the optical domain.

In the central portion of figure 3 and figure 4, the measured values of the static-to-total pressure ratio P/P_T are reported along the nozzle axis. These data are superposed to the ones extracted from a two-dimensional (2D) CFD viscous calculation performed using the SU2 solver and MDM vapor modeled as a polytropic ideal gas ($\mathrm{MDM_{PIG}}$). The ideal specific heat ratio in the temperature range of interest is $\gamma = 1.018$. For the two tests, it is evident that the flow behaves as an ideal gas at maximum $Z_T = 0.98$, being experimental data well captured by the PIG simulation. The bottom part of figure 3 and figure 4 report the compressibility factors Z along the axis, which are computed as a function of the measured static pressure P and of the specific entropy $s = s(P_T, T_T)$ upstream of the nozzle. The compressibility factor decreases as higher non-ideal inlet conditions (lower Z_T) are considered. It increases along the nozzle due to the expansion process. For the $\mathrm{MDM_{PIG}}$ case, instead, a constant value of 1 was obtained for the the computed Z.

The $\mathrm{MDM_{PIG}}$ expansion line can be compared with experimental data for MDM, thus highlighting the non-ideal flow behavior. For both nozzles, the local pressure ratio P/P_T is higher with respect to the ideal-gas counterpart and results to be dependent on inlet conditions, as predicted by theory (see e.g. [32]), thus confirming the non-ideal character of the flow. This behavior is well visible as the expansion proceeds along the nozzle and compressibility

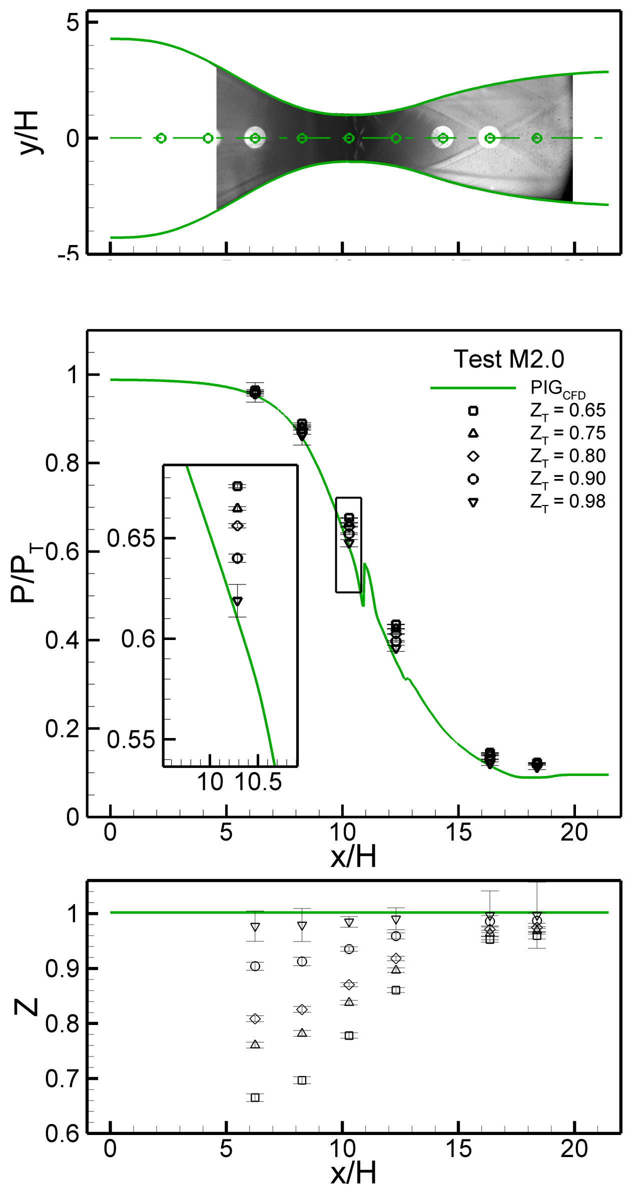

Figure 3: Experimental results for test M2.0. Nozzle non-dimensional geometry (top) overlapped to schlieren images of MDM vapor flow at time $t = 4.75$ s (Z_T=0.70). Throat is located at $x/H = 10.29$. Experimental values at the axis of P/P_T (center) and calculated Z (bottom) as a function of the non-dimensional spatial coordinate x/H at different Z_T. CFD data from viscous calculation coupled with PIG model for MDM are superimposed to the experimental ones.

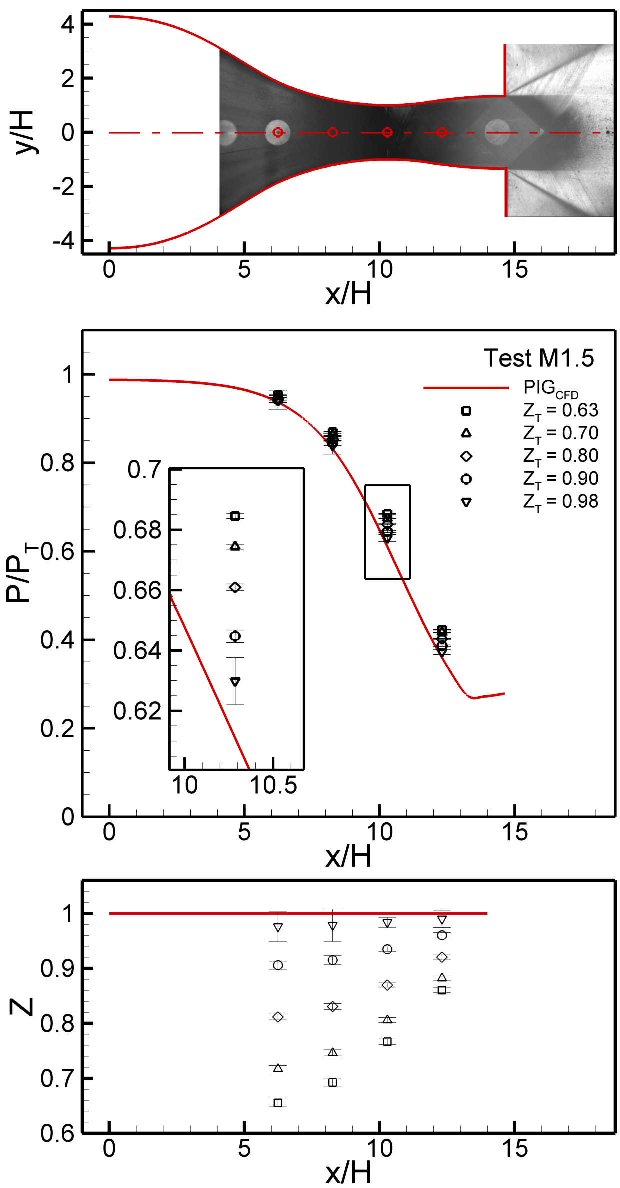

Figure 4: Experimental results for test M1.5. Nozzle non-dimensional geometry (top) overlapped to schlieren images of MDM vapor flow at time $t = 1.60$ s (Z_T=0.65) for test M1.5. Throat is located at $x/H = 10.29$. Experimental values at the axis of P/P_T (center) and calculated Z (bottom) as a function of the non-dimensional spatial coordinate x/H at different Z_T. CFD data from viscous calculation coupled with PIG model for MDM are superimposed to the experimental ones.

effects increase. The departure from the calculated ideal-gas behavior is higher at lower values of Z_T and reduces as dilute gas conditions are approached. This dependence is found to be non negligible at both high and moderate non-ideal states. For instance, taking as a reference the almost perfect gas state ($Z_T = 0.98$), deviations of P/P_T at the geometrical throat are about 6% for $Z_T = 0.80$ and 9% for $Z_T = 0.65$ (referring e.g. to test M2.0).

The departure of the measured data from the ideal gas behavior, with values of P/P_T increasing as more non-ideal conditions are considered, exhibit a trend which is consistent with the one obtained by applying one-dimensional theory for isentropic flows implementing the polytropic van der Waals model, the simplest one taking into account inter-molecular forces responsible for non-ideal gas effects. Quantitatively more accurate predictions are obtained if state-of-the-art non-ideal thermodynamic models are applied, e.g. the improved Peng-Robinson Stryjek-Vera (iPRSV) [33] or the multiparameter Helmoltz energy model implemented in RefProp [21].

Figure 5 reports a comparison between the measured data and the ones extracted at the axis line from a 2D viscous CFD calculation, performed using the SU2 software suite coupled with the thermodynamic and transport models implemented in RefProp [21, 30]. For nozzle M2.0 a profile with no step was used for simulations, due to the local nature of perturbations introduced by the step at the throat. For plot clarity, only data corresponding to maximum and minimum Z_T are reported. Uncertainty bars are also shown to indicate measurements accuracy. For the two nozzles, the computed local pressure ratio P/P_T is in good agreement with the measured one. Deviations are below 7%, except for the exhaust section, where discrepancies tend to slightly increase probably due to boundary-layer effects not properly caught by the 2D simulation. Deviations are indeed not only related to thermodynamic models, but also to transport properties models and to CFD wall treatment. A detailed discussion on the validation of the SU2 suite for simulation of non-ideal compressible flow, including uncertainty quantification, can be found in [14].

4.2. Non-ideal Mach number distribution

For test M1.5, the Mach number was measured at the diverging portion centerline through the detection of Mach waves. These are weak isentropic waves triggered in the supersonic domain by the contoured wall roughness. The wave slope μ relative to the flow direction is only dependent on the local Mach number M (indeed $M = 1/sin(\mu)$). At the centerline the flow velocity is parallel to the axis, due to symmetry. Therefore, the local Mach number can be obtained by measuring the slope of Mach waves detected through schlieren visualizations.

Images of the steady flow field previously analyzed in terms of pressure ratio were extracted and processed in order to provide complementary Mach measurement at different levels of non-ideality. The employed wave detection algorithm requires image decomposition, binarization of image portions extracted at the axis and the application of the Hough transform [34] by which Mach lines are identified. Their slope is finally obtained by implementing the algorithm described in [35]. Expanded uncertainty of Mach measurements U_M is calculated

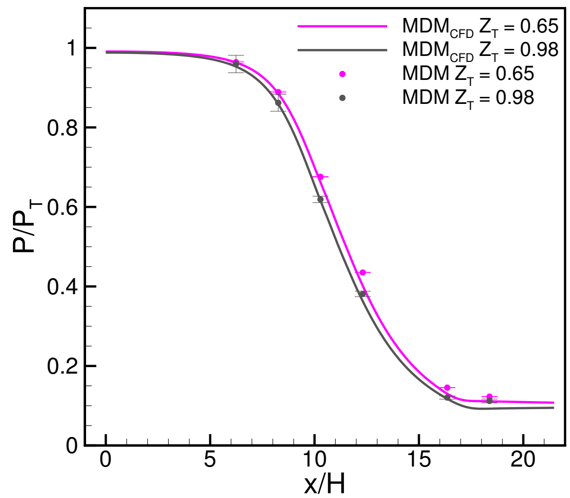

(a) *M2.0*

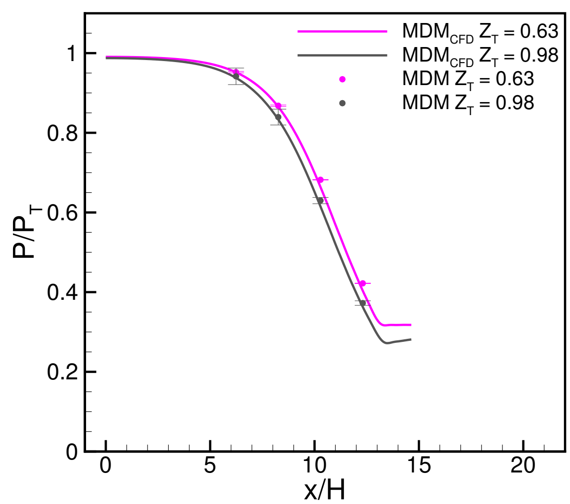

(b) *M1.5*

Figure 5: Comparison between experimental and CFD values of P/P_T at the nozzle axis as a function of x/H for tests M2.0 and M1.5. CFD data are extracted at the axis from a 2D viscous simulation, carried out using the SU2 suite and the RefProp model for MDM. A smooth geometry of nozzle M2.0 was employed for simulations, due to the local nature of the perturbations caused by the recessed step.

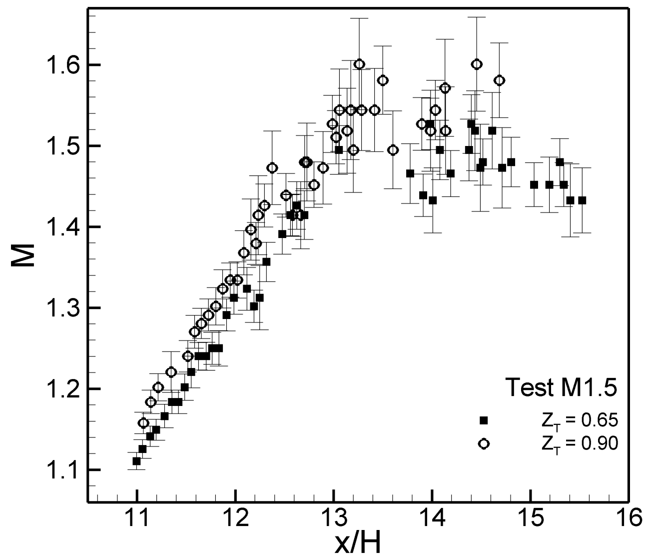

Figure 6: Mach number distribution measured at the axis line of the diverging portion of the nozzle for test M1.5. Data measured at different levels of non ideality, $Z_T = 0.65$ and $Z_T = 0.90$, are compared.

on the basis of angular uncertainty, which is in turn dependent on the camera resolution and on the sub-image dimensions. The position of Mach line end-points is assumed to be described by a probability distribution function which is uniform over the pixel area. The resulting expanded uncertainty is an increasing function of the Mach number (see figures 6 and 7) due to the strong increase of the function $(\sin\mu)^{-1}$; indeed for a given angular uncertainty U_μ, $U_M = M\sqrt{M^2-1}\,U_\mu$.

Figure 6 compares Mach measurements at minimum and maximum Z_T at which readable schlieren images were available for test M1.5. The non-ideal nature of the flow at the axis is confirmed by the dependency of the Mach number on nozzle stagnation conditions. Moreover, the Mach distribution along the axis is consistent with the pressure ratio one. The Mach number indeed decreases as conditions become more non-ideal. The same trend results from the application of one-dimensional theory to steady compressible flows when a non-ideal thermodynamic model (e.g. van der Waals) is applied, see [36].

The top of figure 7a shows a schlieren image of the supersonic flow field in the nozzle diverging portion for test M1.5, extracted at $Z_T = 0.65$. Results of a second test, labeled M1.5' and performed with the same nozzle at $Z_T = 0.81$ are also shown in Figure 7b in order to provide further confirmation of the consistency between measured and calculated data. During test M1.5' two pressure taps were available in the diverging portion, contrarily to test M1.5 where only one tap was active. The nozzle profile and the identified Mach lines

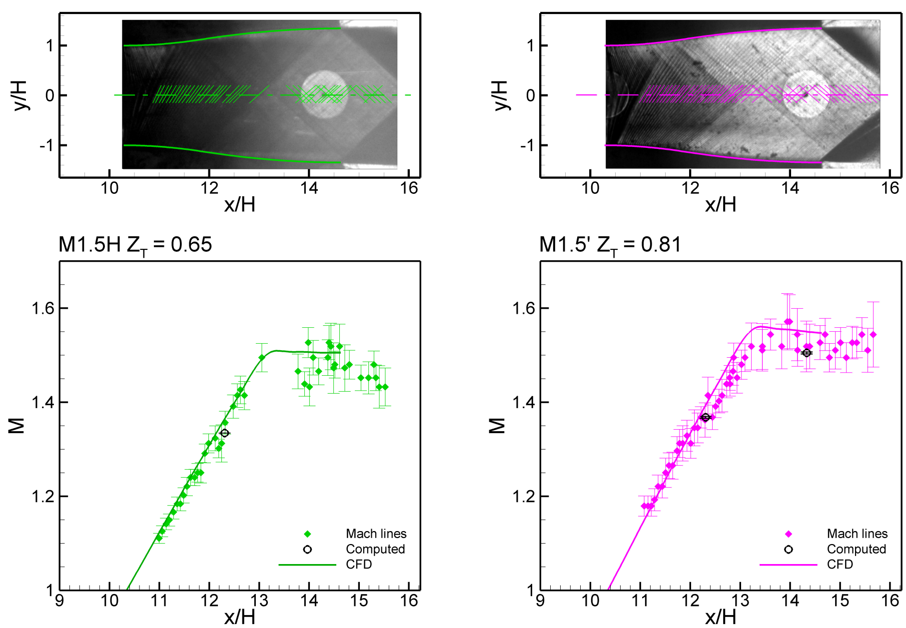

(a) *M1.5* (b) *M1.5'*

Figure 7: Comparison of the Mach number measured through Mach lines, computed through the RefProp model and experimental P, P_T, T_T, and extracted from CFD calculation for test M1.5 at $Z_T = 0.65$ (a) and for test M1.5' at $Z_T = 0.81$ (b). One and two active pressure taps were available in the diverging portion for tests M1.5 and M1.5' respectively.

are also highlighted.

The bottom part of figure 7 provides a comparison between the measured Mach number and the one extracted at the axis line from the previously described CFD simulation. Consistently with pressure ratio comparisons in figure 5, CFD data are within the Mach number uncertainty bars, confirming the accuracy of CFD calculations. Moreover, figure 7 also compares the schlieren-measured Mach number and the one computed at active pressure taps using the RefProp thermodynamic model and the measured pressure and temperature, $M = M(P, s)$ where $s = s(P_T, T_T)$. In this case, deviations between the two dataset are only due to the thermodynamic model. The accordance between computed and measured Mach number is very good, thus providing further proof of the reliability of the multiparameter Helmoltz energy model implemented in RefProp.

In this section, an analysis of the non-ideal effects on nozzle expanding flows of MDM vapor was carried out referring to the local pressure ratio P/P_T and Mach number M along the nozzle axis, so as to only employ quantities directly measured during the experimental campaign. Other properties, such as the speed of sound c, the enthalpy drop Δh, the density ρ, which are relevant for an accurate modeling of the flow, are also influenced by non-ideal effects. These properties can be calculated once a reliable thermodynamic model for the vapor is available. Previous comparison between measured and calculated dataof the nozzle flow field have shown that the state-of-the-art Helmoltz model implemented in RefProp can be considered as reliable. It can therefore be taken as a reference to calculate other flow properties and to assess the accuracy of simpler equations of state that can be employed to model isentropic expansions of MDM vapor, as carried out in the following section.

5. Thermodynamic modeling of non-ideal expansions of MDM vapor

In an early turboexpander design stage, it is required to calculate thermodynamic parameters (such as the isentropic enthalpy drop across an expansion and the outlet-to-inlet volume ratio) that can provide clear indications on machine type and geometry (flow configuration and number of stages). For fluids commonly employed in ORC systems, the use of state-of-the-art thermodynamic models is straightforward and relatively fast, thanks to their implementation in widely available libraries. However, some fluids may not be present in such libraries, and simpler models may be used. Indeed, for the aforementioned preliminary calculations, highly accurate thermodynamic properties are not necessary. In this respect, a suitable model is represented by the van der Waals one, which is simple, general, and easy to implement, especially in its polytropic form. It is therefore interesting to verify the van der Waals model accuracy in order to point out its capability of predicting the architecture of ORC turboexpanders at a preliminary level. As presented in previous sections, the thermodynamic model implemented in the RefProp library (RP) was verified against experimental data to be accurate for the considered fluid and geometry. It is therefore used here as a reference to evaluate to which extent both van der Waals and ideal gas models are suitable for turboexpander preliminary design.

This section presents MDM isentropic expansion modeling in the non-ideal region where the RefProp thermodynamic model was verified through the experimental campaign previously presented. Steady isentropic expansions are computed with different thermodynamic models of increasing complexity: Polytropic Ideal Gas (PIG), Polytropic van der Waals gas (PvdW) and van der Waals gas (vdW). These are all characterized by a simple and fast implementation, with no need of employing external libraries or look-up tables, although they are not always quantitatively accurate. Results for each Equation of State (EoS) are compared with the RP model in order to evaluate the model complexity required for a sufficiently accurate prediction of the non-ideal expansion behavior.

For any given fluid, a steady isentropic expansion is fully defined once the initial thermodynamic conditions, here in terms of pressure P_0 and temperature T_0, and the final state, here in terms of pressure P, are specified. For the present calculations, the initial state is fixed to the most non-ideal one attained in test M2.0, with $P_0 = 9.02$ bar and $T_0 = 269$ °C, corresponding to $P_{0r} = P_0/P_C = 0.63$ and $T_{0r} = T_0/T_C = 0.96$. Different expansions are considered, with a pressure ratio P/P_0 in the range $0.01 < P/P_0 < 1$ or, equivalently, $1 < \beta < 100$, where $\beta = P_0/P$ is the expansion ratio. Ratios of interest for ORC applications are included in this analysis, as well as thermodynamic regions where the fluid behavior is non-ideal. Independently of the component implementing the process, the thermodynamic characterization of an isentropic expansion requires to specify, at any point along the process, properties such as speed of sound c, density ρ (or specific volume $v = 1/\rho$), enthalpy h, and temperature T.

Steady expansions of interest for ORC applications are both those occurring within nozzles (or turboexpander blade rows) and those performed by single or multiple expander stages. In the case of nozzles, the total enthalpy of the flow is conserved and initial conditions are simply stagnation ones $P_0 = P_T$, $T_0 = T_T$, which are constant along the entire isentropic expansion. Therefore, the pressure ratio P/P_T (where P is the static pressure along the expansion) describes the process, since each value corresponds to a specific set of thermodynamic properties (e.g. c, ρ, T, h) and also to a specific nozzle section and Mach number. Relevant quantities for nozzles are indeed also the Mach number M and the quasi-one dimensional critical area ratio A^*/A, where A is the cross sectional area and A^* is the cross sectional area at sonic conditions. In the quasi-1D approximation limit, these flow properties also allow to evaluate the mass flow rate per unit area ρV, where V is the velocity magnitude. If, instead, an expander stage is considered, total conditions change along the expansion due to work extraction. The pressure ratio P/P_0 can be regarded as the stage outlet-to-inlet pressure ratio P_{OUT}/P_{IN}, with no significant distinction between total-to-total or static-to-static ratios.

In order to implement the caloric equation of state for PIG and vdW models, the ideal gas specific heat capacity at constant volume c_V^0 was calculated using the Harrison-Seaton (HS) zero-order method [37], thus avoiding the use of the RefProp model. As noted in [38], HS is the only available technique to estimate ideal gas heat capacities for siloxanes. Group contribution methods cannot be employed because the Si-C bond is not tabulated in literature. The Harrison-Seaton method underestimates c_V^0 with respect to RefProp by about 6% for the considered fluid and temperature range.

For all calculated properties, PvdW and vdW models give almost identical results due to the small variation in c_V^0, which decreases by less than 7% in the temperature range entailed by the considered expansions. For PvdW, c_V^0 is set equal to the one calculated at initial temperature $T_0 = 269$ °C. As expected, vdW is slightly better than PvdW and quantitatively closer to RP.

Figure 8 compares trends of expansion properties for the different analyzed models; percentage deviations from the RefProp model ($\%\Delta_{RP}$) are also plotted.

Speed of sound c and density ρ are shown at the top of figure 8 as a function of the pressure ratio P/P_0 of the expansion. Speed of sound (figure 8a) is poorly represented by the PIG model, with a systematic overestimate that reaches 60% at the highest non-ideal conditions ($P/P_0 \simeq 1$). Also, c is found to decrease along the expansion, opposite to what is predicted by more complex models accounting for intermolecular repulsive and attractive forces. The latter determine an increase in the speed of sound along expansions for the considered fluid and thermodynamic conditions [18]. Both van der Waals models are indeed able to reproduce such trend, but they are quantitatively inaccurate with respect to RP, as they overpredict the speed of sound by a value that can reach almost 12% in the most non-ideal regions at the beginning of the expansion ($P/P_0 \simeq 1$). As it can be seen, the Polytropic van der Waals model and van der Waals model give very similar results, yielding almost indistinguishable trends. Density (figure 8b) is underpredicted by both PIG and vdW models, with higher discrepancies in the most non-ideal regions. The PIG model fails to predict a reasonable value for density, while the vdW deviation is within 10% of RP values.

For nozzle-like expansions, the central portion of figure 8 displays the Mach number M and the critical area ratio A^*/A distribution as a function of the local pressure ratio P/P_T. The PIG model correctly reproduces the Mach number trend (8c), but shows discrepancies that can reach -23%. Both van der Waals models instead show very good accordance with RP, with a percentage difference that is at worst -5%. For instance, the Mach number for a pressure ratio $P/P_T = 0.8$, corresponding to an expansion ratio $\beta = P_T/P = 1.25$, is underestimated by less than 3.5%. Also, the percentage difference with respect to RP is less than 1% in absolute value for $P/P_T \leq 0.5$ ($\beta \geq 2$). These are typical expansion ratios of interest for turbine blade cascades. This result is significant for turbomachinery preliminary design, indicating that a state-of-the-art thermodynamic model is not necessary to estimate the outlet Mach number of a blade cascade and thus to define the outlet flow regime and the blade row type (converging/converging-diverging). The critical area ratio is presented for the four different models in figure 8d. vdW and PvdW have an absolute value of the discrepancy with respect to RP always below 3.5%, whilst PIG can reach

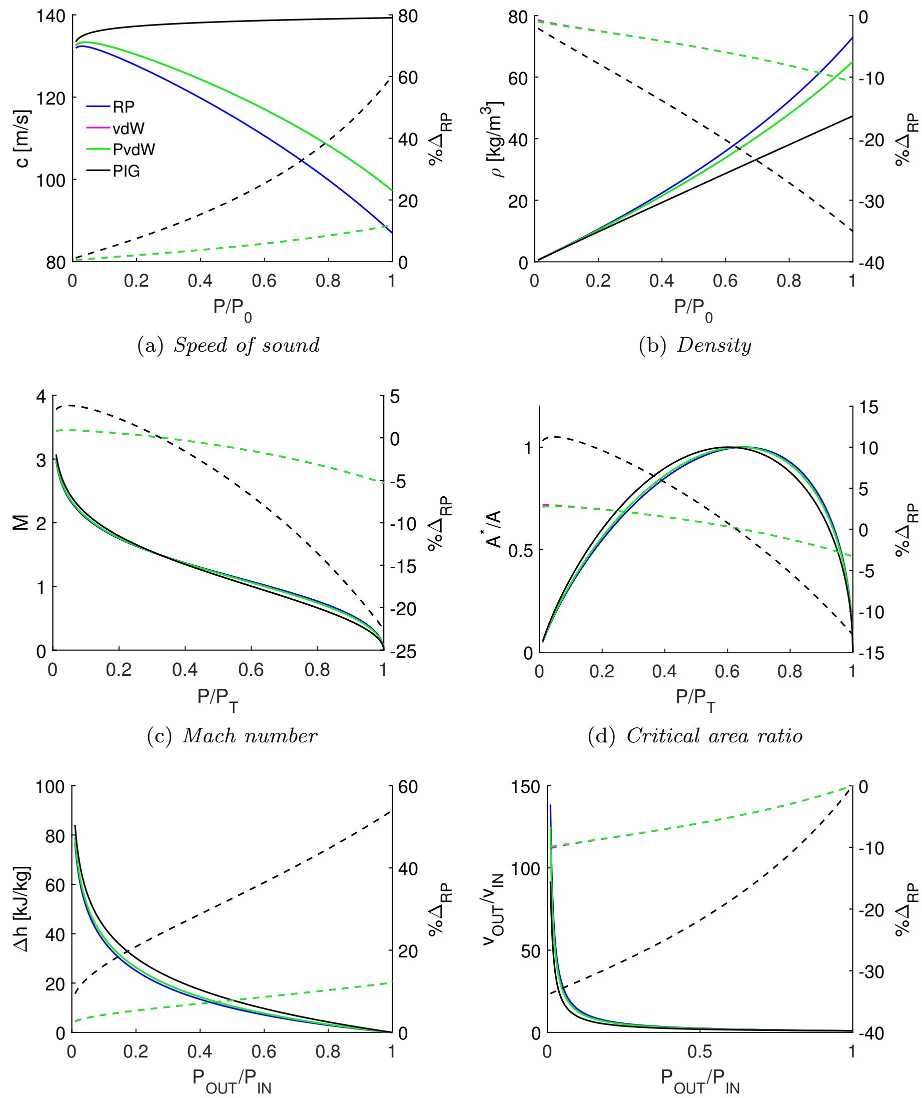

(a) *Speed of sound* (b) *Density*

(c) *Mach number* (d) *Critical area ratio*

(e) *Enthalpy drop* (f) *Volume ratio*

Figure 8: Properties of an isentropic expansion of MDM vapor calculated using different thermodynamic models (solid lines) as a function of the pressure ratio. Initial conditions are $P_0 = 9.02$ bar, $T_0 = 269$ °C and the pressure ratio is in the range $0.01 < P/P_0 < 1$. The percentage difference (dashed lines) is calculated with respect to the RefProp model (RP). Polytropic van der Waals (PvdW) and van der Waals (vdW) models give very similar results, yielding almost indistinguishable trends (the PvdW line always covers the vdW one).

about 12%. The graph also shows that different sonic pressure ratios are predicted depending on the EoS. The PIG model underestimates it by less than 8%, whilst van der Waals models do so by less than 2%. The vdW model can therefore be applied to preliminarily define the cross sectional area of the main section of an expander channel in order to attain the desired expansion ratio.

The T/T_T trend along an expansion, not reported in graphical form for brevity, is fairly well predicted by all models. The PIG EoS has a maximum overestimate with respect to RP of less than 4% and van der Waals models of about 2%. The ratio ρ/ρ_T is poorly predicted by the PIG model, whilst vdW and PvdW overpredict it with respect to RP by less than 10%. The mass flow rate ρV specific to the cross sectional area is evaluated at choked conditions. It is underestimated with respect to RP by about 7.5% by the PIG model and by less than 2.5% by vdW and PvdW models. Such relatively low percentage discrepancy values are due to the fact that the speed of sound is generally overestimated by simpler EoS with respect to RP, whilst density is underestimated; these two aspects compensate each other when the specific mass flow rate is calculated.

For stage expansion processes, the bottom part of figure 8 illustrates the enthalpy drop $\Delta h = h_{IN} - h_{OUT}$ and the volume ratio v_{OUT}/v_{IN} as a function of the outlet-to-inlet pressure ratio P_{OUT}/P_{IN} . The enthalpy drop along the expansion, plotted in figure 8f, is very poorly predicted by the PIG model. Van der Waals models have a maximum difference with respect to RP of about 12% at pressure ratios close to one, when conditions are more non-ideal. For a pressure ratio $P_{OUT}/P_{IN} \leq 0.5$ ($\beta = P_{IN}/P_{OUT} \geq 2$), more typical of a turbine stage, the enthalpy drop is overestimated by less than 8%. This level of accuracy might still be considered as sufficient to determine the stage loading and the number of stages during preliminary turboexpander design. Similarly, the PIG model inaccurately predicts the volume ratio, while both vdW models provide an underestimate that improves with the expansion ratio β, but which is always below 10%, thus allowing a preliminary estimate of the inlet-to-outlet passage area ratio for a stage.

6. Conclusion

The results of detailed experiments, aimed at investigating compressible flows of molecularly complex vapors of interest for ORC power systems, are here reported. These findings extend to more non-ideal thermodynamic conditions the results presented in [17] . The fluid under scrutiny is Siloxane MDM, which is of interest since, due to its high molecular complexity and molecular mass, it is largely and favorably applied in ORCs.

Experimental data are provided for nozzle expansions occurring in highly non-ideal thermodynamic regions. These are fundamental flows in the field of NICFD and are typical in ORC turbine channels. These data are undoubtedly crucial to verify the accuracy of tools employed to model such unconventional flows.

The MDM vapor expanding through two different supersonic nozzles was characterized in terms of stagnation pressure and temperature, of wall static pressure at the axis line, and of density gradient field through schlieren imaging. Inlet conditions ranged from highly non-ideal states to the ideal-gas state, covering a thermodynamic region of typical application for ORC expanders. As expected, the vapor behavior is found to be non-ideal, since the inlet conditions significantly influence the expanding flow, in contrast to the perfect gas case. This proves that taking into consideration non-ideal effects is key in the process of designing and analyzing the performance of ORC turbo-expanders. In this perspective, the accurate predictions of the flow field provided by SU2 suite simulations is also verified.

The performance of simple equations of state for isentropic expansion calculation was evaluated with respect to the state-of-the-art model implemented in RefProp. The van der Waals equation of state was found to have an accuracy level that can be considered acceptable for preliminary ORC turboexpander design, while state-of-the-art thermodynamic models are needed when the accurate design of the expander blade channels is carried out.

Acknowledgements

The research is funded by the European Research Council under ERC Consolidator Grant 2013, project NSHOCK 617603. The initial TROVA layout was funded by Turboden S.r.l..

References

[1] P. Colonna, E. Casati, C. Trapp, T. Mathijssen, J. Larjola, T. Turunen-Saaresti, A. Uusitalo, Organic rankine cycle power systems: From the concept to current technology, applications, and an outlook to thr future, ASME Journal of Engineering for Gas Turbines and Power 137 (2015) 100801–1–19.

[2] E. Macchi, M. Astolfi, Organic Rankine Cycle (ORC) Power Systems. Technologies and applications, Woodhead Publishing Series in Energy: Number 107, Elsevier, New York, 2017.

[3] S. Vitale, G. Gori, M. Pini, A. Guardone, T. D. Economon, F. Palacios, J. J. Alonso, P. Colonna, Extension of the su2 open source cfd code to the simulation of turbulent flows of fuids modelled with complex thermophysical laws, in: 22nd AIAA Computational Fluid Dynamics Conference, no. AIAA Paper 2760, 2015.

[4] M. Pini, G. Persico, D. Pasquale, S. Rebay, Adjoint method for shape optimization in real-gas flow applications, Journal of Engineering for Gas Turbines and Power 137 (3).

[5] G. Persico, M. Pini, V. Dossena, P. Gaetani, Aerodynamics of Centrifugal Turbine Cascades, ASME J. Eng. Gas Turb. Power 137 (112602) (2015) 1–11.

[6] R. Span, W. Wagner, Equations of state for technical applications. i. simultaneously optimized functional forms for nonpolar and polar fluids, International Journal of Thermophysics 24 (1) (2003) 1–39.

[7] P. Colonna, T. P. van der Stelt, FluidProp: a program for the estimation of thermo physical properties of fluids, Software, http://www.FluidProp.com (2004).
URL www.FluidProp.com

[8] M. Pini, A. Spinelli, G. Persico, S. Rebay, Consistent look-up table interpolation method for real-gas flow simulations, Computers and Fluids 107 (2015) 178–188.

[9] T. Mathijssen, M. Gallo, E. Casati, N. R. Nannan, C. Zamfirescu, A. Guardone, P. Colonna, The flexible asymmetric shock tube (fast): a ludwieg tube facility for wave propagation measurements in high-temperature vapours of organic fluids, Experiments in Fluids 56 (10) (2015) 195. doi:10.1007/s00348-015-2060-1.
URL https://doi.org/10.1007/s00348-015-2060-1

[10] A. Spinelli, V. Dossena, P. Gaetani, C. Osnaghi, D. Colombo, Design of a test rig for organic vapours, in: Proceedings of ASME Turbo Expo, Glasgow, UK, 2010.

[11] M. Pini, A. Spinelli, V. Dossena, P. Gaetani, F. Casella, Dynamic simulation of a test rig for organic vapours, in: Proceedings of 5^{th} Conference on Energy Sustainability, ASME EsFuelCell2011, Washington, Washington DC, USA, 2011.

[12] A. Spinelli, M. Pini, V. Dossena, P. Gaetani, F. Casella, Design, simulation, and construction of a test rig for organic vapours, ASME Journal of Engineering for Gas Turbines and Power 135 (2013) 042303.

[13] D. Vimercati, G. Gori, A. Spinelli, A. Guardone, Non-ideal effects on the typical trailing edge shock pattern of orc turbine blades, Energy Procedia 129 (Supplement C) (2017) 1109 – 1116, 4th International Seminar on ORC Power Systems September 13-15th 2017 POLITECNICO DI MILANO BOVISA CAMPUS MILANO, ITALY.
URL http://www.sciencedirect.com/science/article/pii/S1876610217341498

[14] G. Gori, M. Zocca, G. Cammi, A. Spinelli, A. Guardone, Experimental assessment of the open-source su2 cfd suite for orc applications, Energy Procedia 129 (Supplement C) (2017) 256 – 263, 4th International Seminar on ORC Power Systems September 13-15th 2017 POLITECNICO DI

MILANO, MILANO, ITALY.
URL http://www.sciencedirect.com/science/article/pii/S1876610217340171

[15] A. J. Head, C. D. Servi, E. Casati, M. Pini, P. Colonna, Preliminary design of the orchid: a facility for studying non-ideal compressible fluid dynamics and testing orc expanders, Proceedings of ASME Turbo Expo.

[16] F. Reinker, E. Y. Kenig, M. Passmann, S. aus der Wiesche, Closed loop organic wind tunnel (clowt): Design, components and control system, Energy Procedia 129 (2017) 200 – 207, 4th International Seminar on ORC Power SystemsSeptember 13-15th 2017POLITECNICO DI MILANOBOVISA CAMPUSMILANO, ITALY. doi:https://doi.org/10.1016/j.egypro.2017.09.158.
URL http://www.sciencedirect.com/science/article/pii/S1876610217340274

[17] A. Spinelli, G. Cammi, M. Zocca, S. Gallarini, F. Cozzi, P. Gaetani, V. Dossena, A. Guardone, Experimental observation of non-ideal expanding flows of siloxane mdm vapor for orc applications, Energy Procedia 129 (Supplement C) (2017) 1125 – 1132, 4th International Seminar on ORC Power Systems September 13-15th 2017 POLITECNICO DI MILANO, MILANO, ITALY.
URL http://www.sciencedirect.com/science/article/pii/S1876610217341565

[18] P. Colonna, A. Guardone, Molecular interpretation of nonclassical gasdynamics of dense vapors under the van der Waals model, Phys. Fluids 18 (5) (2006) 056101–1–14.

[19] A. Guardone, A. Spinelli, V. Dossena, Influence of molecular complexity on nozzle design for an organic vapor wind tunnel, ASME Journal of Engineering for Gas Turbines and Power 135 (2013) 042307.

[20] A. Spinelli, G. Cammi, S. Gallarini, M. Zocca, F. Cozzi, P. Gaetani, V. Dossena, A. Guardone, Experimental evidence of non-ideal compressible effects in expanding flow of a high molecular complexity vapor, Experiments in Fluids 59 (8). doi:10.1007/s00348-018-2578-0.
URL https://www.scopus.com/inward/record.uri?eid=2-s2.0-85050029437&doi=10.1007%2fs00348-018-2578-0&partnerID=40&md5=0f41ed07e9531ca8c30963e2fe98ea8d

[21] M. Thol, F. Dubberke, E. Baumhgger, J. Vrabec, R. Span, Speed of sound measurements and fundamental equations of state for octamethyltrisiloxane and decamethyltetrasiloxane, Journal of Chemical and Engineering Data 62 (9) (2017) 2633–2648. doi:10.1021/acs.jced.7b00092.
URL https://www.scopus.com/inward/record.uri?eid=2-s2.0-85029502909&doi=10.1021%2facs.jced.7b00092&partnerID=40&md5=49f3275dba830db9f761640c0e20c61d

[22] E. W. Lemmon, M. L. Huber, M. O. McLinden, NIST Standard Reference Database 23: Reference Fluid Thermodynamic and Transport Properties-REFPROP, Version 9.1, National Institute of Standards and Technology (2013).
URL https://www.nist.gov/srd/refprop

[23] P. C. Hung, G. Irwin, R. Kee, S. McLoone, Difference equation approach to two-thermocouples sensor characterization in constant velocity flow environment, Review of Scientific Instruments 76 (024902).

[24] S. Churchill, M. Bernstein, A correlating equation for forced convection from gases and liquids to a circular cylinder in crossflow, Journal of Heat Transfer 99 (2) (1977) 300–306.

[25] S. Whitaker, Forced convection heat transfer correlations for flow in pipes, past flat plates, single cylinders, single spheres, and for flow in packed beds and tube bundles, AIChE Journal 18 (2) (1972) 361–371.

[26] C. Antonini, G. Persico, A. L. Rowe, Prediction of the dynamic respinde of complex transmission line system for unsteady pressure measurament, Measurament Science and Technology 19 (12).

[27] F. Cozzi, A. Spinelli, M. Carmine, R. Cheli, M. Zocca, A. Guardone, Evidence of complex flow structures in a converging-diverging nozzle caused by a recessed step at the nozzle throat, in: 45^{th} AIAA Fluid Dynamics Conference, Dallas, TX, USA, 22-26 June, 2015.

[28] A. Spinelli, F. Cozzi, V. Dossena, P. Gaetani, M. Zocca, A. Guardone, Experimental investigation of a non-ideal expansion flow of siloxane vapor mdm, in: Proceedings of ASME Turbo Expo, Seoul, South Korea, Vol. 3, 2016.

[29] F. Palacios, M. R. Colonno, A. C. Aranake, A. Campos, S. R. Copeland, T. D. Economon, A. K. Lonkar, T. W. Lukaczyk, T. W. R. Taylor, J. J. Alonso, Stanford University Unstructured (SU^2): An open-source integrated computational environment for multi-physics simulation and design, AIAA Paper 2013-0287 51st AIAA Aerospace Sciences Meeting and Exhibit.

[30] T.-H. Chung, M. Ajlan, L. L. Lee, K. E. Starling, Generalized multiparameter correlation for non-polar and polar fluid transport properties, Ind. Eng. Chem. Res. 27 (1988) 671–679.

[31] C. Conti, A. Spinelli, A. Guardone, F. Cozzi, G. Cammi, M. Zocca, Schlieren visualization of non-ideal compressible fluid flows, in: 12th International Conference on Heat Transfer, Fluid Mechanics and Thermodynamics, HEFAT2017, 2017.

[32] H.-S. Tsien, One-dimensional flows of a gas characterized by vander waal's equation of state, Journal of Mathematics and Physics 25 (1-4) (1946) 301–324.

[33] T. van der Stelt, N. Nannan, P. Colonna, The iprsv equation of state, Fluid Phase Equilibria 330 (2012) 24 – 35.

[34] R. O. Duda, P. E. Hart, Use of the hough trasformation to detect lines and curves in pictures, Graphics and Image Processing.

[35] R.-C. Lo, W.-H. Tsai, Gray-scale hough trasform for thick line detection in grey-scale images, Pattern Recognition 28 (1995) 647–661.

[36] P. A. Thompson, A fundamental derivative in gas dynamics, Phys. Fluids 14 (9) (1971) 1843–1849.

[37] B. Harrison, W. Seaton, Solution to missing group problem for estimation of ideal gas heat capacities, Ind. Eng. Chem. Res. 27, 15361540.

[38] P. Colonna, R. Nannan, A. Guardone, E. W. Lemmon, Multi-parameter equations of state for selected siloxanes, Fluid Phase Equilib. 244 (2006) 193–211.